Appl Nanosci (2016) 6:815–825
DOI 10.1007/s13204-015-0493-8

ORIGINAL ARTICLE

Characterization and study of antibacterial activity of spray pyrolysed ZnO:Al thin films

C. Manoharan[1] · G. Pavithra[1] · M. Bououdina[2,3] · S. Dhanapandian[1] · P. Dhamodharan[1]

Received: 28 April 2015 / Accepted: 10 August 2015 / Published online: 21 August 2015

Abstract Aluminum-doped zinc oxide (ZnO:Al) thin films were deposited onto glass substrates using spray pyrolysis technique with the substrate temperature of 400 °C. X-ray diffraction analysis indicated that the films were polycrystalline with hexagonal wurtzite structure preferentially oriented along (002) direction. Surface morphology of the films obtained by scanning electron microscopy showed that the grains were of nanoscale size with porous nature for 6 at.% of Al. Atomic force microscopy observations revealed that the particles size and surface roughness of the films decreased with Al-doping. Optical measurements indicated that ZnO:Al (6 at.%) exhibited a band gap of 3.11 eV, which is lower than that of pure ZnO film, i.e. 3.42 eV. Photoluminescence analysis showed weak NBE emission at 396 nm for Al-doped films. The low resistivity, high hall mobility and carrier concentration values were obtained at a doping ratio of 6 at.% of Al. The effective incorporation of 6 at.% of Al into ZnO lattice by occupying Zn sites yielded a well-pronounced antibacterial activity against *Staphylococcus aureus*.

Keywords Al-doped ZnO · Porous film · Electrical properties · Antibacterial activity

✉ G. Pavithra
gpavithra7@gmail.com

[1] Department of Physics, Annamalai University, Annamalai Nagar, Tamilnadu 608 002, India

[2] Nanotechnology Centre, University of Bahrain, PO Box 32038, Zallaq, Bahrain

[3] Department of Physics, College of Science, University of Bahrain, PO Box 32038, Zallaq, Bahrain

Introduction

Transparent conducting oxides (TCOs) are considered as important basic material for applications in solar cells and optoelectronic devices because of their wide band gap (3.2 eV), low resistivity, high transparency in the visible and near-infrared region, high light trapping characteristics and a high refractive index. Zinc oxide (ZnO) has a quite large binding energy of 60 meV is, which ensures an efficient excitonic emission up to room temperature. In addition, ZnO possesses a high mechanical stability and thermal stabilities. The above unique properties make ZnO a promising material for several technological applications such as ultraviolet/blue emission devices, solar cells, piezoelectric devices, acoustic-optical devices, acoustic resonators, chemical sensors, electro-luminescence displays, heat mirrors (Ghosh and Basak 2013; Bacaksiz et al. 2010) as well as antibacterial activity (Ravichandran et al. 2015). Cuevas et al. (2013) stated that ZnO is a very promising material for the prevention of the food forms being affected by food pathogens such as *Escherichia coli* (*E. coli*) and *Staphylococcus aureus* (*S. aureus*) in the packed foods. Moreover, it can be applied to treat different skin conditions, in products like baby powder and creams against diaper rashes, antiseptic ointments, anti-dandruff shampoos, and as a component in tape (called "Zinc oxide tape") used by athletes as a bandage to prevent soft tissue damage during workouts. Swai et al. (1996) stated that the inorganic compound ZnO exhibits strong resistance against microorganisms. The advantage of using ZnO as antimicrobial agent is due to the fact that its mineral elements are essential to humans and also exhibit strong activity even when asmall amount is administrated into human body.

Pure ZnO films are unstable due to chemisorption and adsorption which modify the surface conductance (Shinde

et al. 2013).The structural, morphological, optical and electrical properties can be effectively modified by doping with a variety of elements like Ga, Al, In, Sn, etc. (Mariappan et al. 2012) . In addition, the incorporation of Group III elements (metal dopants such as Al, In) into ZnO will make the thin films highly conductive which could be the alternative as inexpensive transparent conducting layers for several applications such as transparent display devices, and solar cells. In particular, Al-doped ZnO as transparent conducting oxide (TCO) film offers several advantages over indium tin oxide (ITO) because both elements (Zn and O) are non-toxic and more abundant (Bacaksiz et al. 2010).

Several deposition methods have been used for the preparation of thin films such as sol–gel deposition (Sagar et al. 2005), magnetron sputtering (Czternastek 2008), SILAR (Mondal et al. 2008) chemical bath deposition (Shishiyanua et al. 2005) and spray pyrolysis (Widiyastuti et al. 2012). Among these techniques, spray pyrolysis is the most commonly used one for the preparation of metal oxide thin films due to its simplicity, affordable method with uniform coating, non-vacuum system of deposition and has large area coating with device quality.

To the best of our knowledge, the doping level of ZnO usually has been limited to low concentration. So in the present study it is aimed to enhance the structural, optical and electrical properties of ZnO films doped with Al up to 8 at.% using spray pyrolysis method. Also antibacterial activity against the test organisms is carried out as no antibacterial activity reports are available for Al-doped ZnO films.

Experimental part

Preparation of ZnO:Al thin films

ZnO:Al thin films were deposited onto the microscopic glass substrates by spray pyrolysis technique in air atmosphere from aqueous solutions in which the atomic ratio of Al in the spray solution was varied from 0, 2, 4, 6 and 8 at.%. The substrates were well cleaned prior to deposition by soap solution followed by HCl, acetone and distilled water. Finally, the cleaned substrates were dried in oven. The experimental set-up used for the spraying process consists of a spray head and heater which were kept inside a chamber with an exhaust fan which could remove the gaseous by-products and solvent vapor. The substrate temperature was achieved with the help of heat which is controlled by an automatic temperature controller with an accuracy of ±5 °C. The uniform growth of the films was obtained by moving the spray head in the *X–Y* direction which was able to scan an area of 200 × 200 mm^2 at a speed of 20 mm^{-1} s^{-1} and in steps of 5 mm^{-1} s^{-1} in the *X–Y* plane direction, respectively. In this unit, the flow rate of the solution was controlled by a stepper motor attached to the solution container. The carrier gas used in this experiment was air. The pressure of the carrier gas was maintained with the help of mechanical gauge. The entire unit was connected to computer with the help of a serial port to store the spray parameters. The spray solution was prepared by dissolving 0.1 M of Zn (acac) in ethanol and Aluminum chloride ($AlCl_3$) was added to the solution as a dopant. The prepared solution was sprayed onto glass substrate at the substrate temperature of 400 °C.The grown films were annealed at 500 °C in air for an hour.

Characterization techniques

The structural characterization of the deposited films was carried out by X-ray diffraction (XRD) technique using SHIMADZU-6000 equipped with monochromatic Cu-Kα radiation ($\lambda = 1.5406$ Å). The surface morphology was studied using scanning electron microscope (SEM) JEOL-JES-1600. The surface topology was studied using atomic force microscope (AFM) Nano surf Easy scan 2. Optical absorption spectra were recorded in the range of 300–1200 nm using JASCO V-670 spectrophotometer. The photoluminescence (PL) spectra were recorded at room temperature using prolog 3-HORIBAJOBINYVON with an excitation source wavelength of 375 nm. The electrical resistivity, carrier concentration and mobility were determined by automated Hall Effect measurement ECOPIA HMS—2000 at room temperature in a van der Pauw (VDP) four—point probe configuration.

Antibacterial activity

Preparation of test solution and disc

The test solution was prepared with known weight of fractions in 10 mg/mL, dissolved in 5 % dimethyl sulphoxide (DMSO). Sterile 6 mm discs (Himedia Ltd.) were impregnated with 20 µl of ZnO and Al-doped ZnO (corresponding to 100, 200 and 300 mg/mL) and then allowed to dry at room temperature.

Disc diffusion method

The agar diffusion method (Bauer et al. 1996) was followed for antibacterial susceptibility test. Petri plates were prepared by pouring 20 mL of Mueller–Hinton Agar and allowed to solidify for the use in susceptibility test against bacteria. Plates were dried and 0.1 mL of standardized inoculum suspension was poured and uniformly spread. The excess inoculums were drained and the plates were allowed to dry for 5 min. After drying, the discs with ZnO and Al-doped ZnO were placed on the surface of the plate

with sterile forceps and gently pressed to ensure contact with the agar surface. Gentamycin (30 mg/disc) was used as the positive controls and 5 % DMSO was used as blind control in these assays. Finally, the inoculated plates were incubated at 37 °C for 24 h. The zone of inhibition was observed and measured in millimeters.

Results and discussion

Structural analysis

Figure 1 shows the evolution of X-ray diffraction patterns of undoped and Al-doped ZnO films deposited onto glass substrate. The presence of well-defined peaks confirms the polycrystalline nature of the films, which are identified as (100), (002) and (101) reflections of the hexagonal ZnO crystal structure. The films are in good agreement with those reported in JCPDS data card 36-1451. No additional peaks belonging to other oxides can be detected thereby indicating the formation of pure single ZnO phase, as well as that Al is well incorporated within ZnO lattice.

Pure ZnO thin film exhibits highest intensity for (002) reflection, revealing that the particles (grains) are preferentially oriented along *c*-axis. This is due to the minimal internal stress and surface energy as well as the high atomic density which leads to the easy growth of the crystallites towards the *c*-axis direction. The increase in the intensity of (002) reflection is observed for 1 at.% Al doping. The reduced surface energy due to the substitution of Al at Zn sites leads to more pronounced preferential orientation along (002) plane (Jayakrishnan et al. 2013). This can be also due to the substitution of Zn ions by Al within the hexagonal wurtzite structure, which reduces the surface energy. However, as the doping concentration of Al increases up to 2 at.%, the intensity of (002) plane is decreased, while that of (101) plane increases, indicating a change in growth orientation from *c*-axis into isotropic growth (Liu and Lian 2007). The increase of the intensity of (002), (101) and (100) reflections with increasing doping concentration at 4 at.% indicates the improvement in the crystallinity (Zhang et al. 2008). The intensities of (100) (002) and (101) are further enhanced for 6 at.%, because Al^{3+} ions can easily replace Zn^{2+} ions within ZnO host lattice, as the ionic radius of Al^{3+} (0.53 Å) is smaller than that of Zn^{2+} (0.74 Å). Similar trend of change in orientation from preferred to random orientation of crystallites was observed for Sn-doped ZnO (Tsay et al. 2008). For 8 at.% of Al, the change of growth orientation from (002) to (101) is due to the change in diffusion rate of Zn and O at the surface during deposition, when the presence of Al is excess in the ZnO film (Liu and Lian 2007).

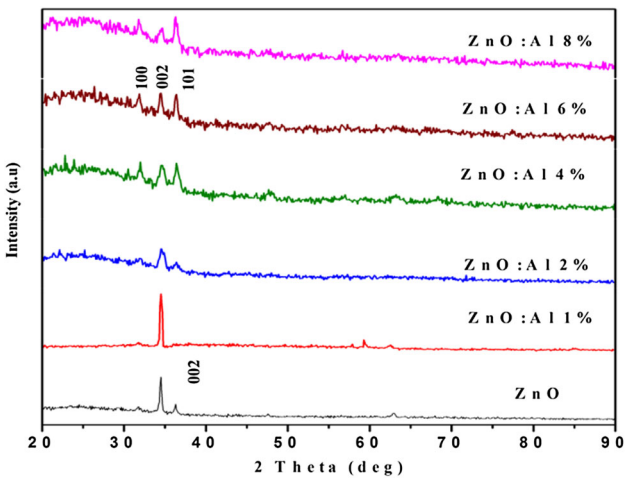

Fig. 1 XRD pattern of undoped ZnO and Al-doped ZnO films

The crystallite size (D) was estimated from peaks broadening using sherrer's equation:

$$D = \frac{k\lambda}{\beta \cos\theta}, \quad (1)$$

where k is a shape factor (0.9), λ is the wavelength of X-rays, β is full width half maximum (FWHM) and θ is the Bragg's angle.

The observed decrease in crystallite size with the increase of Al concentration (Table 1) is due to the stress originated from the difference in the ionic radii between Zn^{2+} and Al^{3+}(r^{2+}_{Zn}:0.074 nm; r^{3+}_{Al}:0.053 nm) or/and a large number of dislocations originated from Al ions occupying interstitial sites within ZnO crystal lattice (Caglar et al. 2012).

The strain (ε) and the dislocation density (δ) were calculated using the following relations:

$$\varepsilon = \frac{\beta \cos\theta}{4} \quad (2)$$

$$\delta = \frac{1}{D^2} \quad (3)$$

From Table 1, it can be noticed that as Al concentration increases both strain and dislocation density also increased, which is due once again to the stress produced by the difference in the ionic radius of Zn and Al (Shinde et al. 2013). The stress of the films is found to be compressive stress as indicated with a negative value, which slightly increases due to the change in the morphology of the film with doping (Rao et al. 2010; Bahedi et al. 2011).

The preferential growth orientation is determined using texture coefficient, $TC_{(hkl)}$, by the following relation:

$$TC_{(hkl)} = \frac{\frac{I_{(hkl)}}{I_{0(hkl)}}}{\frac{1}{n\sum \frac{I_{(hkl)}}{I_{0(hkl)}}}}, \quad (4)$$

where $I_{(hkl)}$ is the measured relative intensity of a plane (hkl), $I_{0(hkl)}$ is the standard intensity of the plane (hkl) taken

Table 1 Strucutral parameters of undoped ZnO and Al-doped ZnO thin films

Sample	$D \times 10^{-9}$ m	$\delta \times 10^{14}$ lines/m^2	$\varepsilon \times 10^{-3}$	σ_{stress} (GPa)	$TC_{(hkl)}$	Lattice parameters Å	
						a	c
Undoped ZnO	38.8208	0.8920	6.6353	−1.155	1.769	3.244	5.201
1 at % Al	49.3606	0.7022	4.1043	−3.536	1.954	3.247	5.206
2 at % Al	13.5647	54.3475	2.5530	−2.688	1.623	3.248	5.205
4 at % Al	12.9618	59.5201	3.6593	−1.849	1.075	3.249	5.200
6 at % Al	10.8382	80.0062	3.1982	−1.192	1.119	3.249	5.179
8 at % Al	7.6030	172.9935	4.5591	−0.796	0.670	3.249	5.165

from the JCPDS data, and n is the number of diffraction peaks. The increase of texture coefficient ($TC_{(hkl)} > 1$) for undoped film shows the preferential orientation of the crystallites along (002) plane. The observed $TC_{(hkl)} \sim 1$ for the film deposited with 4 and 6 at.% of Al shows the change of preferential orientation to random (Mariappan et al. 2012).

The lattice parameters '*a*' and '*c*' for the hexagonal structure can be calculated by the following equation:

$$\frac{1}{d^2} = \frac{4}{3}\left[\frac{h^2 + hk + k^2}{a^2}\right] + \frac{l^2}{c^2} \quad (5)$$

The values of '*a*' and '*c*' (Table 1) are in agreement with the standard values of ZnO single crystal ($a = 3.250$ Å and $c = 5.207$ Å) (Muiva et al. 2011). It can be noticed that the value of '*c*' decreases while that of '*a*' increases significantly. This anisotropic variation in the lattice parameters '*a*' and '*c*' might be probably related to some kind of point defects such as interstitial Al atoms, which leads to the appearance of the crystal growth orientation along (100) and (101) planes as shown in Fig. 1 (Zhang and Que 2010). Moreover, to fulfill charge balance of ZnO, while substituting Zn^{2+} by higher valence Al^{3+}, some vacancies will be created (Zn or/and O). Therefore, the variation of lattice parameters becomes more complicated to discuss, as many factors may contribute simultaneously: Interstitial Al, Substitutional Al, Zn and O vacancies.

Surface morphology

Figure 2 shows SEM images of undoped and Al-doped ZnO thin films. The micrograph of pure ZnO and 1 at.% of Al films depict that the grains are uniformly distributed covering the entire surface area of the substrate and resembles a granular surface. The morphology of 2 at.% Al-doped ZnO exhibits a uniform hierarchical characteristic of grains size. For a doping concentration of 4 at.% of Al, the film exhibits a uniform distribution of spherical grains with compact microstructure. As the Al content further increases up to 6 at.%, the film clearly evidences the absence of close packed morphology and exhibits a porous nature, which is useful for photovoltaic applications (Kaid and Ashour 2007). At much higher doping concentration (8 at.%), the segregation of grains takes place and this is due to the excess of Al content. Therefore, it can be concluded that Al plays a vital role in controlling the morphology of the films.

Composition analysis

The composition of the films is studied by electron dispersive X-ray spectroscopy (EDS). EDS spectra of pure ZnO film (Fig. 3a) confirms the presence of Zn and O in close stiochiometric ratio. The spectrum in Fig. 3b evidences the presence of Al along with Zn and O, where the content of Al is about 3.70 at %, very close to the nominal content.

Surface topography

Atomic force microscopy (AFM) images of pure and 6 at.% Al-doped ZnO thin films are shown in Fig. 4a, b. Figure 4a exhibits granular morphology with a regular arrangement of a hexagonal submicronic aggregates of nanocrystals for pure ZnO film; the average grains size ranges from 80 to 140 nm. From Fig. 4b, it is evident that Al-doped film is formed by large clusters/grains ranging from 150 up to 250 nm due to the agglomeration. The doped film depicts polycrystalline nature, adherent and uniform distribution of grains with small pores. The columnar arrangement of grains seen in 3D image (Fig. 4a) shows the growth along the *c*-axis direction perpendicular to the substrate surface for pure ZnO. This is in agreement with XRD results showing a preferential orientation along (002) plane. The decrease of columnar grains and the formation of island structure of Al-doped film (6 at.%) indicate the deterioration of growth of grains along *c*-axis,

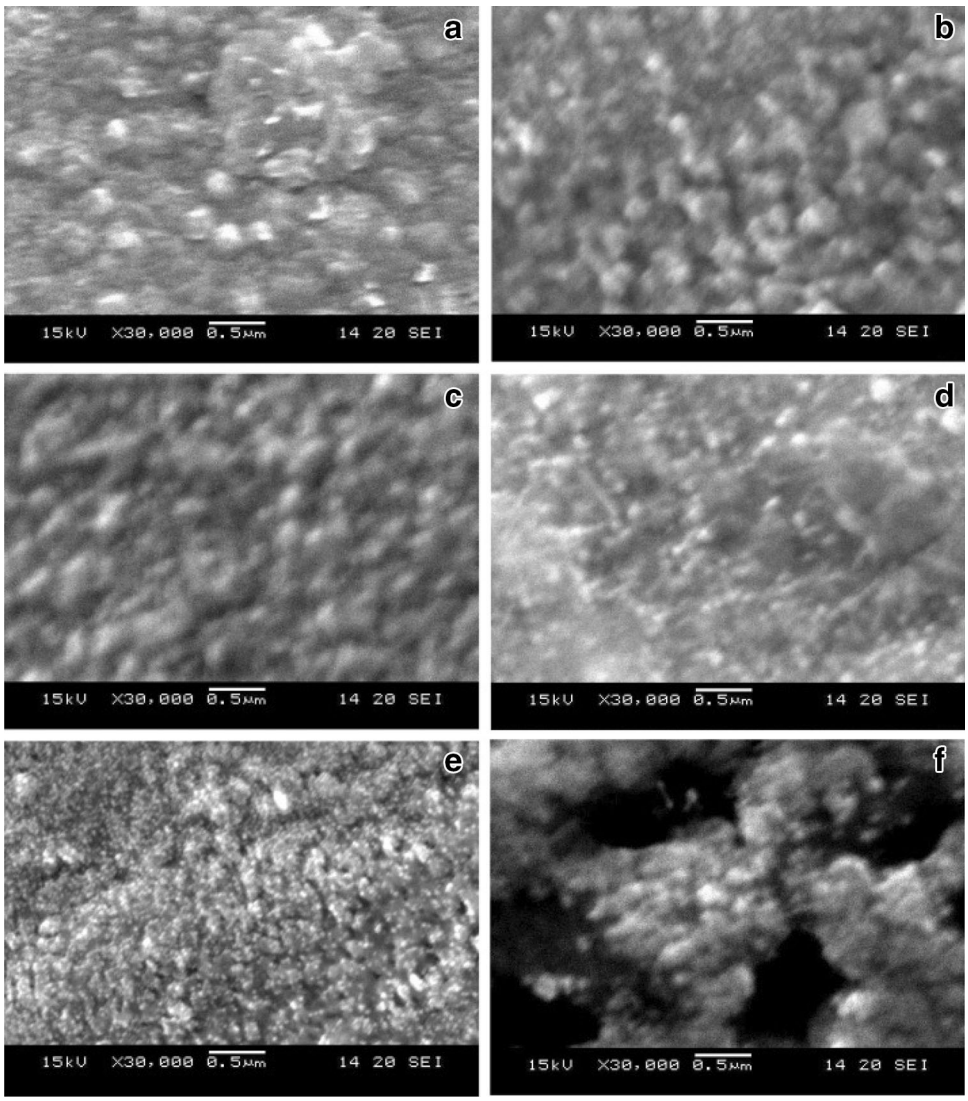

Fig. 2 SEM micrographs for **a** undoped ZnO; **b** 1 at.%; **c** 2 at.%; **d** 4 at.%; **e** 6 at.% and **f** 8 at.% of Al-doped ZnO films

once again in agreement with XRD analysis. The observed surface roughness value of pure and doped films is about 32 and 12 nm, respectively, which shows clearly the decrease of the roughness value with Al doping.

Optical properties

Figure 5 shows UV–vis transmittance spectra of pure ZnO and Al-doped ZnO thin films. The transmittance of all films was found to be low in the UV and high in the visible region. The less scattering effect and structural homogeneity is the reason for the increased transmittance of the films. The transmittance of pure ZnO and 1 at.% of Al-doped ZnO films exhibits nearly 80 % and decreases for higher Al concentrations. Similar trend of increase in transmittance was observed by Shinde et al. (2013) for Sn-doped ZnO. The decrease of transmittance with Al doping may be due to the scattering from pores and other defects present in the film (Shankar et al. 2014).

The optical band gap energy E_g is determined using the following relation:

$$(\alpha hv) = A\left(hv - E_g\right)^n, \quad (6)$$

where E_g is the optical band gap of the films and A is a constant.

Figure 6 shows the plots of $(\alpha hv)^2$ vs (hv) for various ZnO films. The extrapolation of the linear portion of the plot onto the energy axis gives the band gap value. In Fig. 6, the optical band gap decreases from 3.42 up to 3.11 eV with the increase in Al content. This decrease in band gap with increasing Al concentration is attributed to the increase in carrier concentration. Similar result was observed by Ilican et al. (2008), who stated that increasing carrier concentration leads to the band shrinkage with a

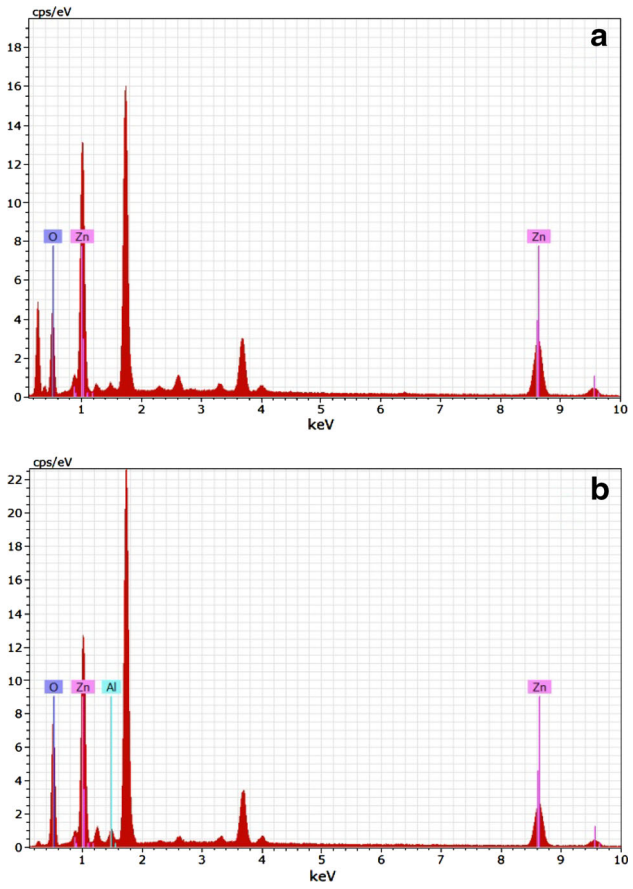

Fig. 3 EDS spectra of **a** undoped ZnO and **b** 6 at.% Al-doped ZnO thin films

shift in the value of the optical band gap. The change in film density and the increase in grain size should be taken into consideration for the decrease in band gap of Al-doped films.

The variation of extinction coefficient (k) and refractive index (n) with wavelength for pure and Al-doped ZnO thin films are shown in the Figs. 7 and 8. In Fig. 7, the extinction coefficient decreases with the increase of wavelength. The variation of absorption can be considered as the main reason for the change in the absorption coefficient. Due to the absorption of light at the grain boundaries, the extinction coefficient decreases. Bhaskar et al. (2001) have also stated that low k value is a qualitative indication of the excellent smoothness of the thin films. The decrease in the extinction coefficient value of Al-doped films indicates a better homogeneity at higher Al concentration (Shanmuganathan et al. 2013). At much higher Al concentration, the extinction coefficient was further increased which is attributed to the appearance of crystal defects (Islam and Podder 2009).

The increase of the refractive index with increasing Al doping concentration may be related to the increase of the compactness of the films. The obtained results show that the refractive index is slightly greater than the refractive index of bulk ZnO (2.0) and then become nearly constant with increasing wavelength (Kaid and Ashour 2007). The similar increment in the refractive index is observed for Er-doped ZnO thin films (Miao et al. 2013). The refractive index of Al-doped film shows a variation up to 2.64 in the visible region which is preferred for antireflection coating materials. Low refractive index was observed for higher Al concentration (8 at.%), which is attributed to the presence of impurities and defects (Islam and Podder 2009)

Photoluminescence (PL) analysis

Figure 9 shows PL spectra of pure and Al-doped ZnO thin films. A strong near-band-edge emission (NBE) was observed for all films. When Al is incorporated into ZnO thin film, it is found that the NBE peak has an emission at 393 nm. A shift of the peak position towards lower wavelength is observed in NBE for Al-doped films with increasing Al concentration (Zi-qiang et al. 2006). The UV emission band is originated from the free exciton recombination. The enhancement of PL intensity by doping with 1 at.% of Al can be attributed to the improvement of the crystallinity as observed from XRD patterns and also to the charge compensation due to the presence of Al (Anandhi et al. 2013).The increase in the intensity of NBE emission observed for pure ZnO and 1 at.% Al-doped ZnO films originates from lesser defects or/and preferred orientation along (002) (Chen et al. 2009). The decrease in PL intensity for Al concentrations above 2 at.% reflects a possible lattice distortion or the formation of new phases (small amount of impurities that cannot be detected within the resolution of the X-ray diffractometer) due to higher Al doping (He et al. 2010). The absence of green emission shows the decreased oxygen vacancies and the improved crystallinity (Anandhi et al. 2013).

Electrical studies

Hall Effect measurements were investigated to study the electrical properties of pure and Al-doped ZnO thin films. It is well known that ZnO is a non-stoichiometeric material having n-type conductivity due to the presence of oxygen vacancies and interstitial Zn atoms. The incorporation of Al^{3+} ions within ZnO crystal lattice by occupying Zn^{2+} sites, Al interstitial atoms, oxygen vacancies and Zn interstitial atoms may be considered as the main reason for the enhanced of electrical conductivity of ZnO. The concentration of free charge carriers in ZnO would be increased by Al doping because Al (Al^{3+}) has one valence electron more than Zn (Zn^{2+}). Pure ZnO film exhibits a resistivity of 1.27×10^3 Ω cm and a carrier concentration of 7.25×10^{14} cm^{-3}. When Al is introduced into ZnO

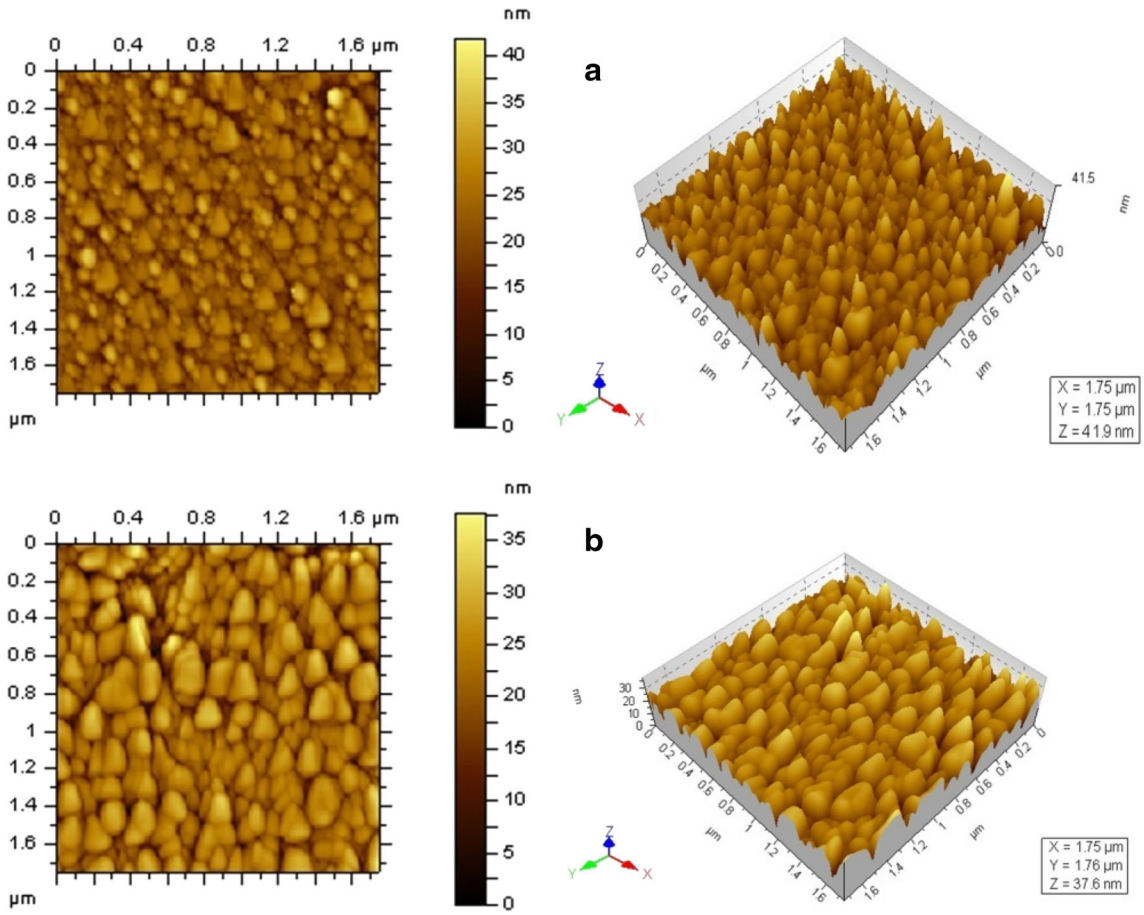

Fig. 4 AFM image of **a** undoped ZnO and **b** 6 at.% of Al-doped ZnO thin films

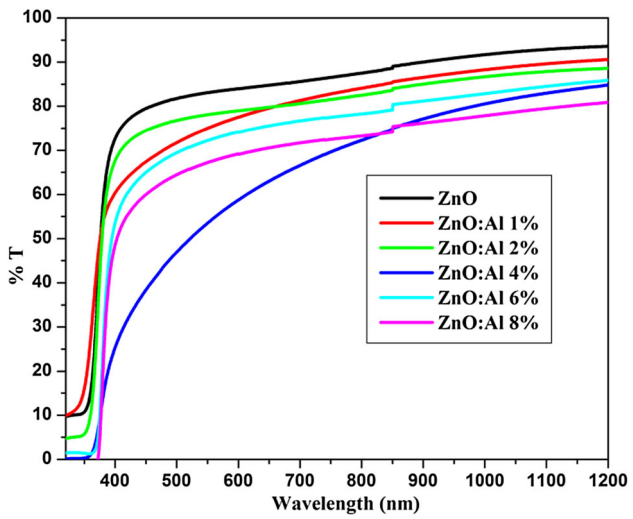

Fig. 5 Optical transmittance of undoped ZnO and Al-doped ZnO thin films

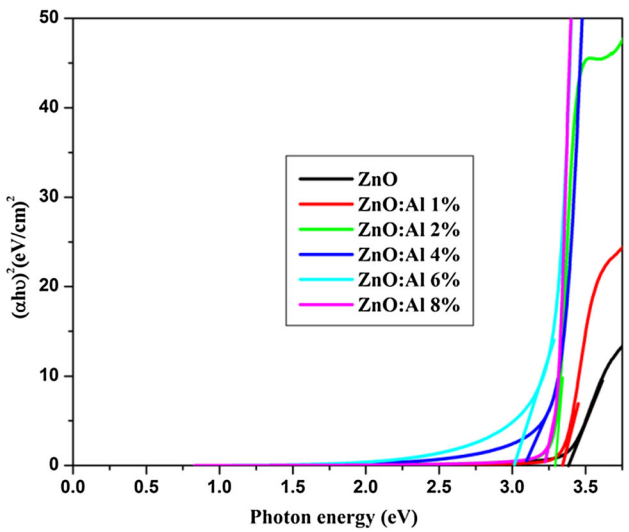

Fig. 6 Variation of $(\alpha hv)^2$ vs hv of undoped ZnO and Al-doped ZnO thin films

film, Zn^{2+} ions get replaced by Al^{3+} ions. Thus one free electron is produced when Zn atom is replaced and hence carrier concentration is increased with a decrease in resistivity (Caglar et al. 2012). The observed resistivity and carrier concentration for 6 at.% of Al is 1.58×10^{-3} Ω cm and 1.56×10^{20} cm^{-3}, respectively. The obtained Hall

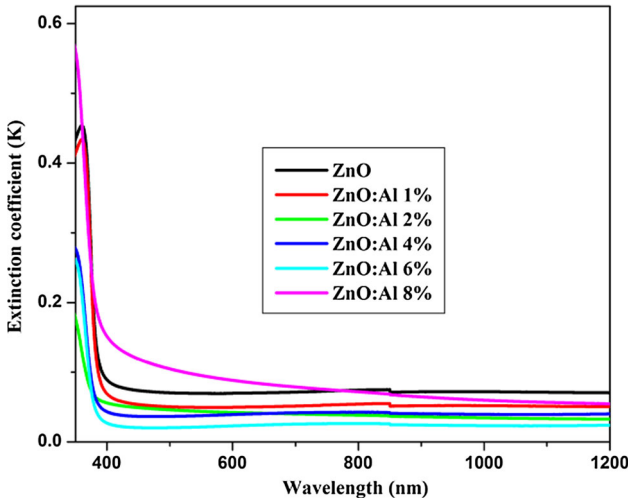

Fig. 7 The variation of extinction coefficient of undoped ZnO and Al-doped ZnO thin films with wavelength

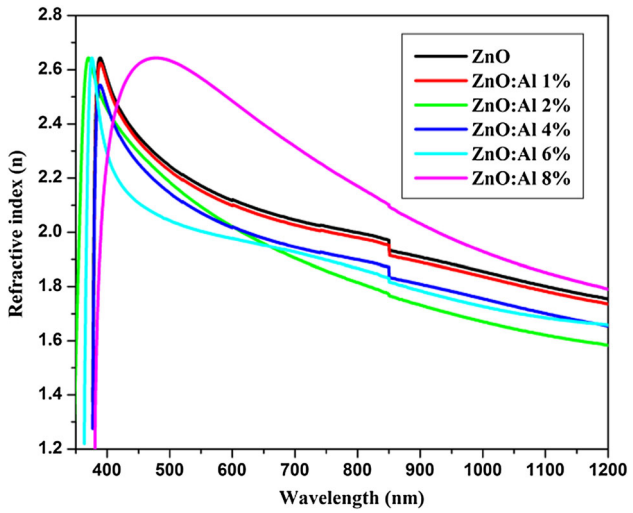

Fig. 8 The variation of refractive index of undoped ZnO and Al-doped ZnO thin films with wavelength

mobility of the undoped and 6 at.% of Al-doped ZnO films is 6.4 and 25.20 cm^2/Vs, respectively.

Antibacterial activity

Figure 10 and Tables 2 and 3 show the antibacterial activity of pure ZnO and 6 at.% of Al-doped ZnO films. The antibacterial activity of pure ZnO in different concentrations against bacteria (*S. aureus*, *K. pneumonia*, *P. aeruginosa*, *P. mirabilis* and *B. subtilis*) is observed. The antibacterial activity was determined based on an inhibition zone. No zone of inhibition was observed for the negative control. Gentamycin is a positive control, for which the zone of inhibition ranges from 13 to 29 mm. The highest mean zone of inhibition (12 mm) is recorded for pure ZnO

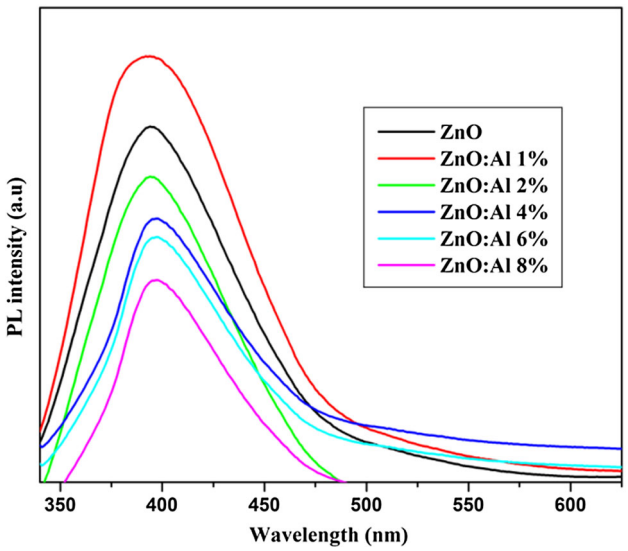

Fig. 9 Photoluminescence emission spectrum of undoped ZnO and Al-doped ZnO thin films

against *S. aureus*, followed by *K. pneumonia* (9 mm), *B. subtilis* (8 and 10 mm)in Table 2 which clearly indicates the mechanism of the biocidal action of the ZnO that destroys the outer of the bacteria leads to the death (Thomas et al. 2014). The observed difference in the diameter of the inhibition zone may be due to the difference in the susceptibility of the different bacteria to the prepared ZnO particles (Bindhu and Umadevi 2015).

Table 2 reveals that the moderate effect of antibacterial activity against *K. pneumonia* (300 mg/mL) and *B. subtilis* (200 mg/mL and 300 mg/mL) can be attributed to the weak attachment of ZnO particles towards the cell wall membrane of the bacteria resulting in the minimization of the formation of the reactive oxygen species (ROS) such as H_2O_2 which are responsible for the inhibition of the building elements of the bacteria (Ekthammathat et al. 2014). As can be seen from Table 2, the maximum antibacterial activity of ZnO was against *S. aureus*. This is because of the firm attachment of ZnO particles to the outer cell wall membrane of the bacteria. After that, ZnO particles begin to release oxygen species into the medium (bacteria), which will inhibit the growth of cell leading to the distortion and leakage of the cell and finally the death of the cell (Ekthammathat et al. 2014).

From Table 3, it is evident that Al-doped ZnO (for all concentrations) showed antibacterial activity not only against S.sureus but also against *K. pneumonia* and *B. subtilis*. Al-doped ZnO showed high sensitivity of antibacterial activity against *S. aureus*. The mean zone of inhibition ranging between 10 and 13 mm is noticed for *S. aureus*. The highest mean zone of inhibition (13 mm) is recorded against *S. aureus* for 6 at.% Al (Table 3).

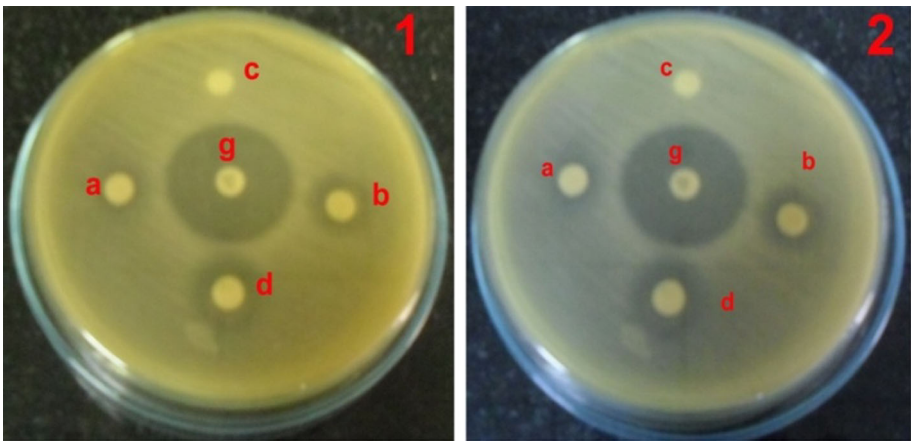

Fig. 10 Antibacterial activity of **1)** undoped ZnO and **2)** 6 at.% of Al-doped ZnO thin films with *g* positive control, *c* negative control, *a* 100 mg/ml, *b* 200 mg/ml and *d* 300 mg/ml against *Staphylococcus aureus*

Table 2 Antibacterial activity of undoped Zinc oxide

Organisms	Zone of inhibition (mm)				
	Control	Gentamycin 30 mg	ZnO (mg/mL)		
			100	200	300
Staphylococcus aureus	NZ	29	8	11	12
Klebsiella pneumonia,	NZ	18	NZ	NZ	9
Pseudomonas aeruginosa,	NZ	13	NZ	NZ	NZ
Proteus mirabilis	NZ	21	NZ	NZ	NZ
Bacillus subtilis	NZ	21	NZ	8	10

Table 3 Antibacterial activity of Al-doped Zinc oxide

Organisms	Zone of inhibition (mm)				
	Control	Gentamycin 30 mg	Al-doped ZnO (mg/mL)		
			100	200	300
Staphylococcus aureus	NZ	29	10	10.5	13
Klebsiella pneumonia,	NZ	18	8.5	9	10
Pseudomonas aeruginosa,	NZ	13	NZ	NZ	8
Proteus mirabilis	NZ	21	NZ	NZ	7.5
Bacillus subtilis	NZ	21	9	8.5	8

The high sensitivity of *S. aureus* may be due to the doped particles which possess the appropriate size and shape of the particles. The particles with smaller size can easily penetrate and interacts into the medium. The interacted particles get accumulated into the medium in large amount and slowly affect the growth of the bacteria which leads to the death of the bacteria. Ragupathi et al. (2011) have reported that small particles of Sn-doped ZnO have a tendency to slow down the bacterial growth. Similar behavior was observed in the present study which is due to the decreased particle size with the increase in Al concentration. During the interaction of the particle with the surface of the cell wall membrane of the bacteria, the generation of oxygen species takes place on the surface. This leads to the cleavage and elongation of the cell wall resulting from the hindering of the growth and multiplication of building elements such as DNA.

The increased liberation of Zn^{2+} from ZnO matrix due to the substitution of Al plays a major role in the mechanism of antibacterial activity by producing reactive oxygen species. This reactive oxygen species can kill the bacteria directly by penetrating the membrane. The antibacterial activity against *P. aeruginosa* and *P. mirabilis* shows no zone formation for 100 mg/mL and 200 mg/mL of

Al-doped ZnO which states that the material has no effective antibacterial effect, whereas at higher concentration 300 mg/mL of Al-doped ZnO against *P. mirabilis*, *B. subtilis*, the zone of inhibition was 8 and 10 mm, respectively. This shows that at this concentration, Al ions might have a minor influence on the bacteria.

Conclusion

Pure and Al-doped ZnO films were deposited by spray pyrolysis technique using ZnAcAc and $AlCl_3$ as precursor solution. Nanocrystalline hexagonal structure was revealed by XRD with a preferred orientation along (002) up to 2 at.% of Al and random for higher doping level. SEM observations revealed that the films were dense with uniform surface coverage on the substrate except for 6 at.% of Al. The elemental composition determined by EDS confirmed the presence of Zn, O and Al. AFM analysis showed a change from columnar structure (*c*-axis orientation) into spherical nature (random orientation) for Al-doped films. The surface roughness of Al-doped ZnO films was found to be around 12 nm, which is much smaller compared with pure ZnO, i.e. 32 nm. The deposited films showed excellent transparency and the band gap decreased with increasing Al concentration. All the films exhibited high transmittance and low absorbance in the visible/near infrared region, thus making the films suitable for optoelectronic devices and window layers in solar cells. According to PL study, the absence of green emission indicated that the concentration of oxygen vacancy-related defects was lower in pure ZnO and Al-doped ZnO films. The carrier concentration and Hall mobility were increased for Al-doped films. Therefore, it is evident from the above observations that 6 at.% Al-doped ZnO thin film can be used as electrode once it is deposited onto ITO-coated glass plate in the fabrication of solar cell. Furthermore, antibacterial activity results indicated that 6 at.% of Al-doped ZnO yielded the high antibacterial activity against *S. aureus,* thus reflecting excellent anti-bacterial effect and potential in reducing bacterial growth for practical applications.

Acknowledgments The authors are grateful to the University Grants commission, New Delhi, India, for the financial support through research Grant No. 42-860/2013 (SR).

References

Anandhi R, Ravichandran K, Mohan R (2013) Conductivity enhancement of ZnO:F thin films by the deposition of SnO2:F over layers for optoelectronic applications. Mater Sci Eng B 178:65–70

Bacaksiz E, Aksu S, Yılmaz S, Parlak M, Altunbaş M (2010) Structural, optical and electrical properties of Al-doped ZnO microrods prepared by spray pyrolysis. Thin Solid Films 518:4076–4080

Bahedi K, Addou M, El Jouad M, Sofiani Z, Oauzzani HE, Sahraoui B (2011) Influence of strain/stress on the nonlinear-optical properties of sprayed deposited ZnO:Al thin films. Appl Surf Sci 257:8003–8005

Bauer AW, Kirby WMM, Sherris JC, Turek M (1996) Antibiotic susceptibility testing by a standardized single disc method. Am J Clin Phothol 45:493–496

Bhaskar S, Majumder SB, Jain M, Dobal PS, Katiyar SR (2001) Studies on the structural, microstrucutral and optical properties of sol-gel derived lead lanthanum titanate thin films. Mater Sci Eng B 87(2):178–190

Bindhu MR, Umadevi M (2015) Antibacterial and catalytic activities of green synthesized silver nanoparticles. Spectrochim Acta Part A Mol Biomol Spectrosc 135:373–378

Caglar Y, Caglar M, Ilican S (2012) Microstructural, optical and electrical studies on sol gel derived ZnO and ZnO:Al films. Curr Appl Phys 12:963–968

Chen KJ, Hung FY, Chang SJ, Hu ZS (2009) Microstructures, optical and electrical properties of In-doped ZnO thin films prepared by sol–gel method. Appl Surf Sci 25:6308–6312

Cuevas AG, Balangcod K, Balangcod T, Jasmine A (2013) Surface morphology, optical properties and antibacterial activity of zinc oxide films synthesized via spray pyrolysis. Proced Eng 68:537–543

Czternastek H (2008) Effect of deposition geometry on structural, electrical and optical properties of ZnO:Al films by magnetron sputtering. Vacuum 82:994–997

Ekthammathat N, Thogtem S, Thongtem T (2014) Characterization and antibacterial activity of nanostrucutred ZnO thin films synthesized through a hrdrothermal method. Anukorn Phuruangrat Powder Technol 254:199–205

Ghosh T, Basak D (2013) Enhanced mobility in visible-to-near infrared transparent Al-doped ZnO films. Sol Energy 96:152–158

He X, Dong W, Zheng F, Fangang L, Shen M (2010) Effect of tartaric acid on the microstructure and photoluminescence of $SrTiO_3$:-Pr^{3+} phosphorous prepared by a sol-gel method. Mater Chem Phys 123:248–288

Ilican S, Caglar Y, Caglar M, Yakuphanoglu F (2008) Structural, optical and electrical properties of F-doped ZnO nanorod semiconductor thin films deposited by sol–gel process. Appl Surf Sci 255:2353–2359

Islam MR, Podder J (2009) Optical properties of ZnO Nano fibre thin films grown by spray pyrolysis of Zinc Acetate precursor. J Cryst Res Technol 44:286–292

Jayakrishnan R, Mohanachandran K, Sreekumar R, Kartha CS, Vijayakumar KP (2013) ZnO thin films with blue emission grown using chemical spray pyrolysis. Mater Sci Semicond Process 16:326–331

Kaid MA, Ashour A (2007) Preparation of ZnO-doped Al films by spray pyrolysis technique. Appl Surf Sci 253:3029–3033

Liu Y, Lian J (2007) Optical and electrical properties of aluminum-doped ZnO thin films grown by pulsed laser deposition. Appl Surf Sci 253:3727–3730

Mariappan R, Ponnuswamy V, Suresh P (2012) Effect of doping concentration on the structural and optical properties of pure and

tin doped zinc oxide thin films by nebulizer spray pyrolysis (NSP) technique. Superlatt Microstruct 52:500–513

Miao L, Tanemura S, Zhao L, Xiao X, Zhang XT (2013) Ellipsometric studies of optical properties of Er-doped ZnO thin films synthesized by sol–gel method. Thin Solid Films 543:125–129

Mondal S, Kanta KP, Mitra P (2008) Al-doped ZnO (AZO) thin film by SILAR. J Phys Sci 12:221–229

Muiva CM, Sathiaraj TS, Maabong K (2011) Effect of doping concentration on the properties of aluminium doped zinc oxide thin films prepared by spray pyrolysis for transparent electrode application. Ceram Int 37:555–560

Ragupathi KR, Koodali RT, Manna AC (2011) Size-dependent bacterial growth inhibition and mechanism of antibacterial activity of zinc oxide nanoparticles. Langmuir 27:4020–4028

Rao TP, Santhosh Kumar MC, Safarulla A, Ganesan V, Barman SR, Sanjeeviraja C (2010) Physical properties of ZnO thin films deposited at various substrate temperatures using spray pyrolysis. Phys B 405:2226–2231

Ravichandran K, Rathi R, Baneto M, Karthika K, Rajkumar PV, Sakthivel B, Damodaran R (2015) Effect of Fe + F doping on the antibacterial activity of ZnO powder. Ceram Int 41:3390–3395

Sagar P, Kumar M, Mehra RM (2005) Electrical and optical properties of sol–gel derived ZnO:Al thin films. Mater Sci-Poland 23–30:685–696

Shankar S, Saroja M, Venkatachalam M, Balachander M, Kumar V (2014) Influence of Al concentration on structural and optical properties of Aluminum doped zinc oxide thin films prepared by sol gel spin coating method. J Nano Sci Nano Technol 2:769–772

Shanmuganathan G, Shameem Banu IB, Krishnan S, Ranganathan B (2013) Influence of K-Doping on the optical properties of ZnO thin films grown by chemical bath deposition method. J Alloy Compd 562:187–193

Shinde SS, Korade AP, Bhosale CH, Rajpure KY (2013) Influence of tin doping onto structural, morphological, optoelectronic and impedance properties of sprayed ZnO thin films. J Alloy Compd 551:688–693

Shishiyanua ST, Lupan OI, Monaicoa EV, Ursakib VV, Shishiyanua TS, Tiginyanu IM (2005) Photoluminescence of chemical bath deposited ZnO:Al films treated by rapid thermal annealing. Thin Solid Films 488:15–19

Swai J, Kawada E, Kanou F, Igarishi H, Hashimoto A, Kokung T, Shimizu M (1996) Detection of oxygen generated from ceramic powders having antibacterial activity. J Chem Eng Jpn 29:627–633

Thomas D, Abraham J, Vattappalam SC, Augustine S, Dennis Thomas T (2014) Antibacterial activity of pure and cadmium doped ZnO thin film. Indo Am J Pharma Res 4:1612–1616

Tsay C-Y, Cheng H-C, Tung Y-T, Tuan W-H, Lin C-K (2008) Effect of Sn-doped on microstructural and optical properties of ZnO thin films deposited by sol gel method. Thin Solid Films 517:1032–1036

Widiyastuti W, Setiawana A, Winardi S, Nurtono T, Madhaniaa S, Susanti D (2012) The influence of Al dopant precursors on the characteristics of ZnO fine particles prepared by ultrasonic spray pyrolysis. Proc Eng 50:152–158

Zhang J, Que W (2010) Preparation and characterization of sol–gel Al-doped ZnO thinfilms and ZnO nanowire arrays grown on Al-doped ZnO seedlayer by hydrothermal method. Sol Energy Mater Sol Cells 94:2181–2186

Zhang W, Zhu S, Li Y, Wang F (2008) Photo catalytic Zn- doped TiO_2 films prepared by DC reactive magnetron sputtering. Vacuum 82:328–335

Zi-qiang X, Hong D, Yan L, Hang C (2006) Al-doping effects on structure, electrical and optical properties of *c*-axis-orientated ZnO:Al thin films. Mater Sci Semicond Process 9:132–135